Journal of Catalysis 425 (2023) 203–211

Contents lists available at ScienceDirect

Journal of Catalysis

journal homepage: www.elsevier.com/locate/jcat

Research article

Limitations of free energy diagrams to predict the catalytic activity: The reverse water gas shift reaction catalyzed by Ni/TiC

Pablo Lozano-Reis [a,*], Hector Prats [b,*], Ramón Sayós [a], Francesc Illas [a]

[a] Departament de Ciència de Materials i Química Física & Institut de Química Teòrica i Computacional (IQTCUB), Universitat de Barcelona, C. Martí i Franquès 1, 08028 Barcelona, Spain
[b] Department of Chemical Engineering, University College London, Roberts Building, Torrington Place, London WC1E 7JE, UK

ARTICLE INFO

Article history:
Received 10 March 2023
Revised 24 May 2023
Accepted 27 May 2023
Available online 1 June 2023

Keywords:
Surface coverage
kinetic Monte Carlo
Density Functional Theory
Kinetic modeling
Mechanistic analysis
Rational design
Reverse water-gas shift reaction

ABSTRACT

The temporal evolution at the catalyst surface is a result of an intricate interplay between all involved microscopic events such as adsorption, desorption, diffusion, and bond breaking/formation steps, and the interaction with the surrounding environment. By properly including these effects, kinetic Monte Carlo (kMC) simulations can accurately describe the complexity of real catalysts, unravel the dominant reaction mechanisms and provide fundamental understanding towards the rational design of novel catalysts. In this work, we combine density functional theory (DFT) calculations, statistical thermodynamics and kMC simulations to study the reverse water–gas shift (RWGS) reaction on Ni/TiC, a bifunctional catalyst. The predictions from DFT energy profiles do not coincide with the outcome of the kMC simulations, evidencing the limitations of the former, especially in including the effect of coverage of surface species, which plays a crucial role. The kMC simulations results are in remarkable agreement with the experimental data, proving that the kMC simulations are able to describe the complex chemistry of the RWGS reaction on a bifunctional catalyst.

1. Introduction

Experimentally, it is extremely challenging to understand why a given material can be highly active towards a particular reaction, which is crucial for a rational design of novel catalysts. This is, in part, because of the high complexity of real industrial catalysts, which typically involves metal clusters or nanoparticles supported over some substrate with many active regions that are exposed to the incoming reactants [1]. Moreover, many industrial reactions encompass a large number of adsorbed species and elementary steps that take place simultaneously. Despite notable progress in the use of experimental *operando* techniques [2–8], a detailed description of the active sites and dominant reaction path is still out of reach. The rational design of efficient catalysts is generally unfeasible without a clear guidance from theoretical modeling, ideally going from the atomic and molecular level to the macroscopic scale. Quantum mechanical calculations, most often in the framework of Density Functional Theory (DFT), provide useful insights into the molecular reaction mechanism, such as the energetics of the different adsorbates and transition states involved, which allow for the construction of the potential energy surfaces (PES), usually approximated investigating each elementary step separately, or Gibbs free energy diagrams at temperature and pressure conditions of interest. The obtained profiles are often used to unveil the most plausible path, at least from a static point of view. Note, however, that rigorously speaking one should consider pre-exponential factors as relying on energy barriers only can be misleading. Nevertheless, the information provided from the electronic structure calculations, hereafter assumed to rely on DFT, is generally insufficient to correctly determine the time evolution and thus to disclose the dominant reaction mechanism [9,10]. This is particularly the case for reactions involving many elementary steps and/or complex catalysts facing different active regions. In fact, the coverage of different species involved in a heterogeneously catalyzed reaction can be extremely important in determining the time evolution under working conditions to the point that it may not be possible to predict the catalytic activity or unveil the dominant reaction pathway along time from solely DFT calculations, except perhaps for simple systems.

To bridge the gap between the static picture at the atomic level and the macroscopic regime, DFT calculations must be coupled with kinetic modelling techniques [11–14] that capture adsorbate mobility (diffusion), steric exclusion effects, complex reaction patterns involving adsorbates in specific binding configurations,

* Corresponding authors.
E-mail addresses: p.lozano@ub.edu (P. Lozano-Reis), h.garcia@ucl.ac.uk (H. Prats).

https://doi.org/10.1016/j.jcat.2023.05.026
0021-9517/

spatial correlations arising from adsorbate lateral interactions and changes in the energy barriers due to the presence of neighboring spectator species. These effects can be modelled by means of kinetic Monte Carlo (kMC) simulations and used in this work to illustrate that the conclusions extracted from DFT energy diagrams are in complete disagreement with the outcome of kMC simulations. This is illustrated taking the case of the reverse water–gas shift (RWGS) reaction ($CO_2 + H_2 \rightarrow CO + H_2O$) on Ni/TiC. The choice of this system comes from a series of recent works, where transition metal carbides (TMCs) have been shown to be active supports for small metal clusters, presenting a catalytic activity and selectivity much superior to the same particles dispersed on more traditional oxide supports [15], a result of the strong polarization of the electron density of the supported particles [16,17]. For instance, small Ni particles dispersed on TiC are able to dissociate CH_4 at room temperature [18] and displays a catalytic activity towards the RWGS reaction that is two orders of magnitude higher compared to that of the clean TiC(001) surface [19]. Preliminary DFT calculations suggested that the overall CO production was dominated by the Ni cluster [20], but the underlying chemistry responsible for this boost of catalytic activity is, however, not totally understood, as it involves a network of elementary steps taking place in three distinct regions: the supported Ni cluster, the bare TiC region, and the interface region that lies in the middle.

Here, we combine DFT calculations with kMC simulations to study the RWGS reaction on the complex Ni/TiC catalyst. The DFT derived PES suggests that the catalytic activity decreases in the order Ni > interface > TiC. However, the kMC simulations show a completely opposite trend, with the TiC region being the most active one, and the Ni region almost acting as a mere spectator. This surprising result is directly related to the key role of surface coverage and site blocking, an aspect that cannot be captured from DFT calculations only. Even more, the kMC simulations explain why the Ni/TiC catalyst is more active than the bare TiC surface, even if the TiC region is the active one which, again, is attributed to coverage effects. Remarkably, the present kMC simulations not only correctly capture the relative increase in turnover frequency (TOF) between Ni/TiC and TiC but predict a TOF absolute value in close agreement with experiment [19]. This work reaffirms the importance of kinetic studies beyond the analysis of DFT energy barriers or (free) energy profiles, and highlights the fundamental role played by the surface coverage of the different adsorbates, which tends to be ignored.

2. Methods

DFT Calculations. To characterize the energetics of the RWGS reaction on Ni/TiC, spin polarized periodic DFT calculations using the BEEF-vdW functional [21] have been carried out by means of the Vienna Ab Initio Simulation Package (VASP) code [22–24]. An appropriate supercell (Fig. 1a) has been used to represent the three different regions of the TiC system: the supported Ni cluster (Ni region), the interface between the Ni cluster and the TiC support (interface region), and the bare TiC surface (TiC region). Because all three regions are catalytically active, we have computed the formation energies for the different adsorbates and properly characterized transition states, which are needed for the subsequent kMC simulations, as well as quantifying the energy barriers for diffusion steps and the lateral interactions between adsorbates. In addition, Gibbs free energy profiles are presented which permit to account for temperature and pressure effects. The free energy profiles are obtained following the procedure outlined by Nørskov *et al.* [25]. Further details on the used computational setup and how formation energies and lateral interactions are calculated can be found in Section S1, S2 and S3 in the Supporting Information, respectively. Note that the choice of 4 atoms for the Ni cluster is because experiments suggests the active particles to be small (few atoms) and 2D [19], and subsequent computational studies confirmed the high activity of Ni_4 clusters for the CO_2 and H_2 activation [20]. Morevoer, this particular size features a compact, high symmetry structure that maximizes the atomic coordination with *fcc* TiC and is thus highly likely to be energetically stable.

Kinetic Monte Carlo simulations. The simulations have been carried out using the graph-theoretical kMC approach [26] combined with cluster expansion Hamiltonians [27,28] for the surface energetics as implemented in the Zacros code (version 3.01) [26,27]. The kMC lattice model (Fig. 1b) is built so as to mimic the slab model used for the DFT calculations (Fig. 1a), and consists of a 4×4 periodic custom grid of 68 points— or a total of 1088 points— representing surface sites, where the different species can adsorb, desorb, react or diffuse. A total of 8 different site types have been used, as described next. For the TiC region, surface C and Ti atoms are represented by tTi and tC sites. For the interface region, C atoms are represented by tC_{in} sites and the two different types of Ti atoms are represented by $tTi_{in\text{-}1NN}$ and $tTi_{in\text{-}2NN}$, where 1NN and 2NN stand for 1st-nearest neighbors and 2nd-nearest neighbors, respectively. Mapping the DFT calculations, all C and Ti sites can be occupied by monodentate species, such as CO adsorbed on tC, or multidentate species such as HCOO occupying two neighboring tTi sites. The supported Ni_4 cluster is represented by a single coarse-grained lattice site labeled as Ni. This special choice is made because most adsorbed species occupy the whole Ni_4 cluster. By using a single Ni site instead of four Ni sites, the use of many tridentate and tetradentate species is avoided, simplifying the input files. For the few cases in which two species are simultaneously adsorbed on the supported cluster, we make use of double labels; in this way, $OH+OH^{Ni}$ label represents two OH species coadsorbed on the Ni_4 cluster. Finally, to avoid the use of a "hard sphere" model for small adsorbates like H and H_2, we use special hydrogen reservoir sites [29]; h and h_{Ni} for those H or H_2 species far and near the Ni_4 cluster, respectively. We must point out that the convergence with respect to lattice size has been verified by computing the steady state TOFs at larger lattice sizes, finding no significant difference (Table S1).

The reaction network involves a total set of 82 reversible reactions, including adsorption, desorption, diffusion and surface reaction steps. The huge number of elementary reactions arises from the heterogeneity of the Ni/TiC model and from the possibility of having the different elementary steps occurring with both reactants/products at the same region, or in different regions with a concomitant change on the energetics. Obviously, the casuistic has been explicitly contemplated on the DFT calculations and transferred to the kMC simulations. The cluster expansion used in our model includes pairwise lateral interactions between all possible reactant/product pairs as well as all other relevant species and has been truncated to 1NN two-body terms, although some 2NN two-body terms have also been included. Overall, it contains 40 one-body terms and 105 two-body terms, which are summarized in Table S2 and S3 in the Supporting Information. Making use of the cluster expansion and of the Brønsted-Evans-Polanyi relations is it possible to capture the effect that local reaction environment has on the coverage-dependent energy barriers which is crucial to properly describe the temporal evolution on the catalyst surface [30–33]. The difference in time scales of all processes has been handled by manual scaling of the transition probabilities of the fastest processes by some scaling factor $\alpha < 1$ to speed up the kMC simulations while ensuring that this does not affect the final results. This pragmatic solution has been previously applied in several studies [29,34–37].

We have considered an initial mixture of CO_2 and H_2 continuously impinging on an initially empty surface, in which different

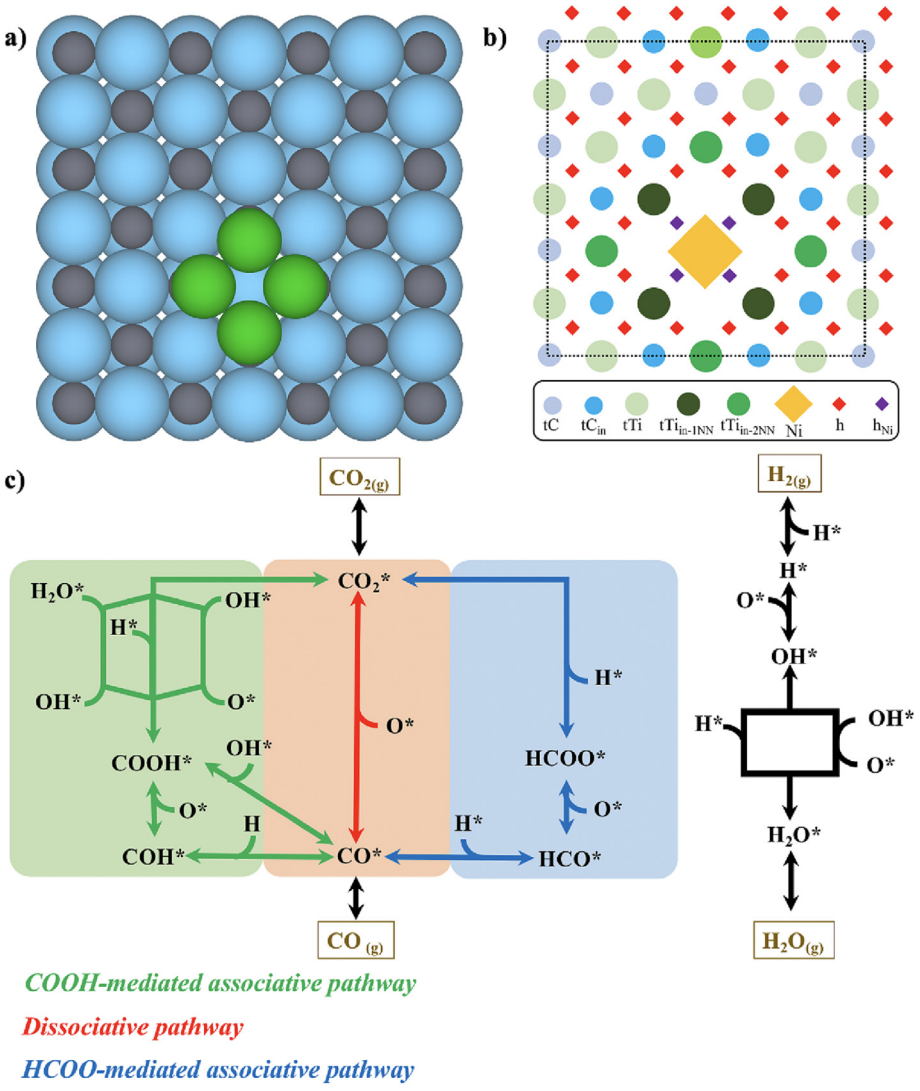

Fig. 1. a) Unit cell for the Ni/TiC surface model used on the DFT calculations. Grey, light blue and green represent C, Ti and Ni atoms, respectively. b) Lattice model used for the kMC simulations of the Ni/TiC model. Black dashed lines show the unit cell. c) Possible reaction pathways of the RWGS reaction. (For interpretation of the references to colour in this figure legend, the reader is referred to the web version of this article.)

surface processes can take place, and afterward, the formed products can desorb and leave the surface without allowing for subsequent re-adsorption. The working conditions are chosen as in the experiments by Rodriguez *et al.* [19], which are: P(H_2) = 4.5 bar and P(CO_2) = 0.5 bar and temperatures ranging from 500 K to 600 K. All the simulations have been run until at least 1000 molecules of CO have been produced under steady state conditions. For each operating condition, we have run 5 different simulations that differ from each other only in the sequence of random numbers used. Therefore, the overall macroscopic properties here reported correspond to an average of the production stage of five independent kMC simulation replicas. The kMC setup used for the clean TiC model is summarized in Section S4. From the results of the kMC simulations, we obtain *(i)* the event frequencies of the different processes, defined as the number of times an event is executed per unit time and area (the TOF is therefore the event frequency for CO or H_2O desorption); and *(ii)* the site occupancy for each adsorbate species in each site type, defined as the average number of labels of a particular adsorbate (or dentates in the case of multidentate species) on a particular site type divided by the total number of sites of that type. The site occupancy is therefore a measure of the surface coverage.

3. Results

3.1. The static atomistic picture.

In principle, the reasons why the RWGS activity on Ni/TiC is two orders of magnitude higher than on TiC can be obtained from inspecting the PES. More in detail, by locating the relevant stationary points corresponding to reactants, intermediates, products and the transition states between them. The RWGS reaction mechanism can proceed either through the dissociative (CO_2* dissociation) or associative (COOH* or HCOO* formation) pathways as shown in Fig. 1c. Let us start by considering the associative mechanisms. From the energy barriers listed in Table S4, it appears that one can consider just the COOH* intermediate because the HCOO* intermediate is generally harder to form simply because COOH* formation is favored on the TiC and interface regions while HCOO* formation is only preferred over the Ni region. Results in Table S4 also suggest that the COOH formation always occurs through CO_2* reacting with H* and not with OH*. For each region in the Ni/TiC catalyst, we focus now on the dissociative (CO_2*→ CO*+O*) and the COOH-mediated associative (CO_2*+H*→ COOH*→ CO*+OH*) pathways. In the TiC region, the free energy diagram in Fig. 2a, at

the specified realistic conditions, suggests that the dissociation pathway, with a barrier of 1.03 eV, probably dominates. The COOH* formation step, despite having a quite low barrier of 0.80 eV, is very uphill, resulting in a reverse energy barrier from COOH* back to CO_2* of 0.31 eV only. Moreover, bimolecular steps such as COOH* formation are limited by the availability of reactants and therefore less likely to occur than unimolecular ones. In the interface region, the free energy diagram indicates that the dissociative pathway clearly dominates, with an energy barrier of 0.72 eV compared to the 1.02 eV barrier for COOH* formation as shown in Fig. 2b. This is also the case for the supported Ni cluster (Fig. 2c), where the energy barriers for CO_2* dissociation and COOH* formation are 0.54 and 1.42 eV, respectively. From this information one would conclude that the RWGS reaction activity of the different regions increases in the order TiC < interface < Ni; this is following the trend of the energy barriers for CO_2 dissociation— 1.03, 0.72 and 0.54 eV for TiC, interface, and Ni, respectively— as shown in Fig. 2d. Therefore, the analysis of the DFT derived free energy diagram suggests that the dissociative pathway is the dominant reaction mechanism; and that the higher activity of Ni/TiC for the RWGS reaction, compared to TiC, is mainly due to the superior ability of the Ni cluster (and the interface, to a lower extend) to break CO_2* compared to the TiC region. In the next section, we will show why this is a largely oversimplified picture.

3.2. Accounting for kinetics and going to macroscopic scale leads to surprises

One may naively think that the outcome of a kinetic study is just to complement the picture arising from the analysis of the PES, bringing details concerning conversion at given conditions of pressure and temperature. This implies accepting that the conclusions from the static picture hold when going to a macroscopic scale, when temperature and pressure are properly defined. While this may be the case for simple model systems with few elementary steps and no different regions, it is not at all the case here where the system under study closely resembles a real catalyst. In fact, the present kMC simulations, carried out with rates derived from the same DFT calculations, show that almost all CO is produced over the TiC region— 98 % at 500 K and 89 % at 600 K— mainly following the COOH-mediated associative pathway, and the remaining CO is produced at the interface (see TOF values in Fig. 3a). This is in clear contradiction with the activity order and dominant reaction mechanism extracted from the analysis of the DFT PES. A careful inspection of the kMC simulation results shows that the coverage effects along with site availability are responsible for this mismatch between DFT predictions and kMC results, as explained in detail below. In other words, when the catalyst starts to be populated the picture obtained from a single reaction breaks down.

To further support the claims above it is enough to see that, at the initial stage of the simulations (see Fig. 3b), CO_2 adsorbs and dissociates over the Ni cluster, producing O* on the interface and CO* on the cluster which further diffuses to the interface and desorb. Next, H_2 adsorbs and dissociates over the Ni cluster to produce H* that hydrogenates the O* species to produce OH* at the cluster. Then, attractive adsorbate–adsorbate interactions between OH* and neighboring H*, CO_2* and O* species make the OH*+OH* → H_2O*+O* reaction over the Ni cluster very endothermic (Figure S1), with the concomitant cluster poisoning with OH* species, while hindering the adsorption of other species on the cluster. Meanwhile, CO_2 adsorbs at the interface and dissociates producing CO* and more O* at the interface sites. The produced CO* desorbs while most of the O* adatoms remain on the interface, creating a partial poisoning of that region. CO_2 can still be adsorbed at the interface

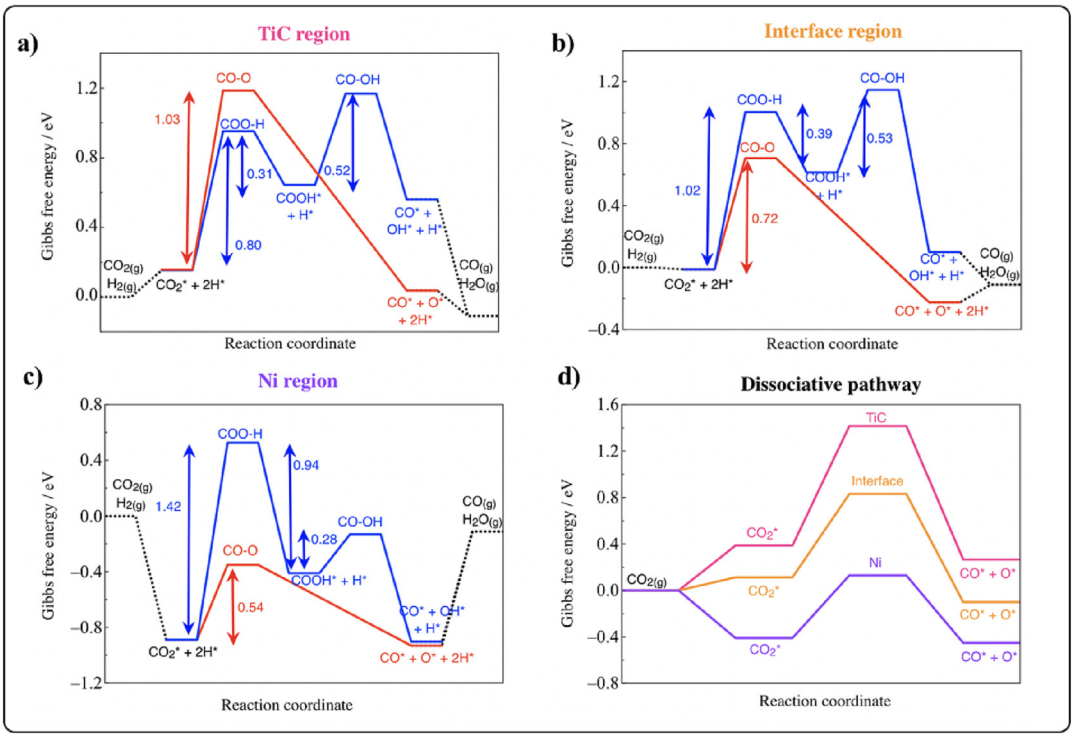

Fig. 2. Gibbs free energy diagrams at T = 550 K and P(CO_2) = 0.5 bar, P(H_2) = 4.5 bar, P(CO) = 0.001 bar and P(H_2O) = 0.001 bar for the dissociative (red) and the COOH-mediated associative (blue) pathways in a) the TiC region; b) the interface region; and c) the Ni cluster. d) Gibbs free energy profiles for CO_2 adsorption and dissociation over the Ni cluster, the interface region and TiC region (purple, orange, and pink lines, respectively). (For interpretation of the references to colour in this figure legend, the reader is referred to the web version of this article.)

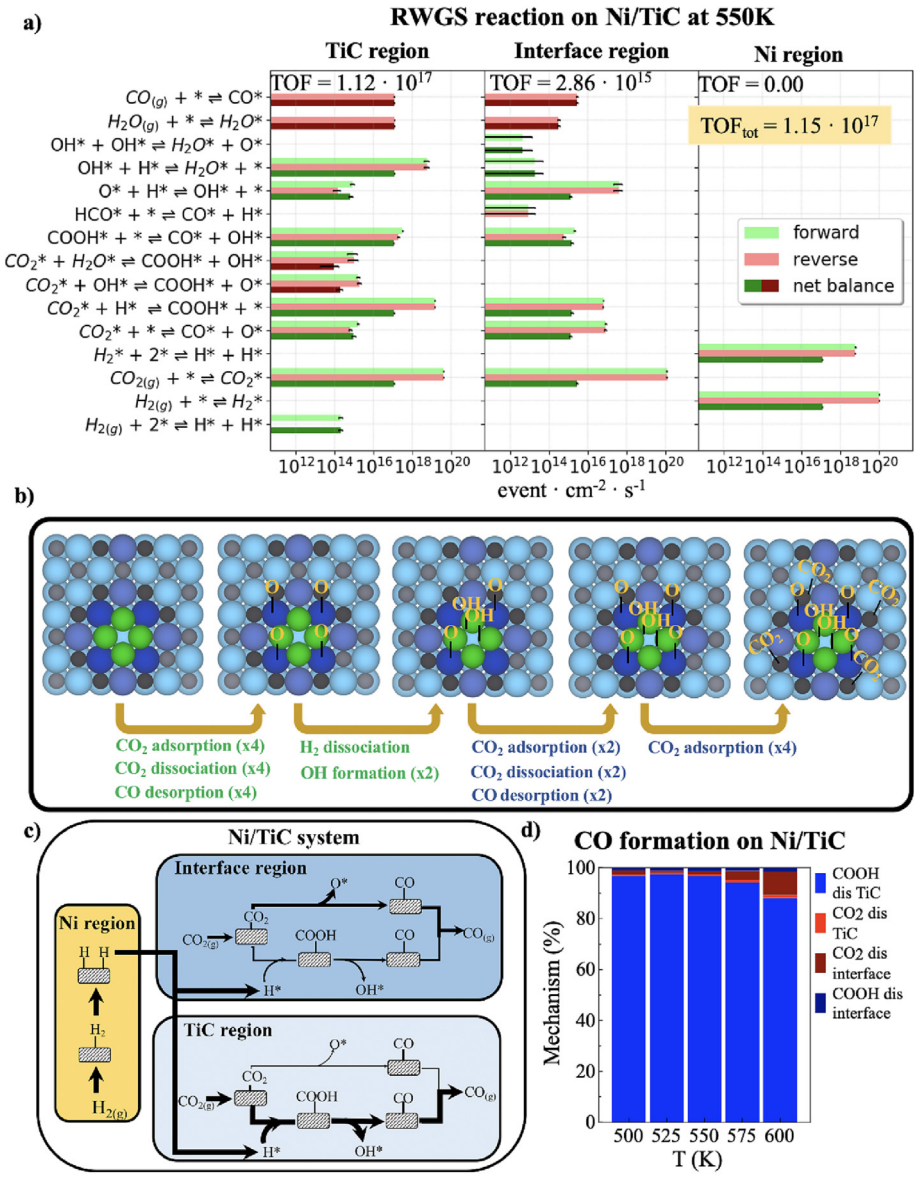

Fig. 3. a) Event frequency of the RWGS reaction on Ni/TiC at T = 550 K and P(H_2) = 4.5 bar and P(CO_2) = 0.5 bar at the different regions. b) Cluster and interface poisoning at the initial stages of the kMC simulations. c) Scheme of the observed mechanism for Ni/TiC model with the role of each region of the catalyst. d) Percentage of the dissociative and COOH-mediated pathways on the final CO production at five different temperatures.

region, but it cannot dissociate due to the site blocking produced by the O* atoms at the interface. Table 1 shows that, at the steady state, all Ni sites are poisoned by OH*, while the interface is partially poisoned by O*. Therefore, the RWGS reaction at steady state conditions occurs almost entirely at the TiC region contrary to what one can infer from the DFT potential energy surface. This

Table 1
Percentage of site occupancy for the different species that are adsorbed on the surface of the Ni/TiC model catalyst at 550 K under steady state conditions. Values of 0.0 represent an occupation lower than 0.05 % while dashes (-) means that this species cannot adsorb at that site.

T = 550 K	Site occupancy (%)							
Species	**tC**	**tTi**	**tC_{in}**	**$tTi_{in\text{-}1NN}$**	**$tTi_{in\text{-}2NN}$**	**Ni**	**h**	**h_{Ni}**
H_2O^*	–	0.1	–	–	0.0	0.0	–	–
COOH*	0.0	0.0	0.0	–	0.0	0.0	–	–
CO*	1.7	–	0.0	–	0.0	0.0	–	–
O*	12.8	–	5.0	89.0	0.1	0.0	–	–
CO_2^*	11.9	59.6	49.3	–	98.5	0.0	–	–
OH*	–	0.8	–	–	0.0	0.0	–	–
OH*+OH*	–	–	–	–	–	100.0	–	–
H*	–	–	–	–	–	–	34.8	50.2
H_2^*	–	–	–	–	–	–	–	2.4
Total	26.4	60.5	54.3	89.0	98.6	100.0	34.8	52.6

unexpected and interesting phenomenon can only be captured by kMC simulations, which naturally accounts for the effect of surface coverage.

At this point, one could argue that it is also possible to include coverage effects in the PES by performing the pertinent energy barrier calculations at a chosen coverage, thus improving the accuracy of the prediction from the PES. This possibility, however, becomes unpractical when the structure of the adlayer under operating conditions is unknown and the number of possible combinations of adsorbates in the neighboring sites is very high, as it is the case for the RWGS on Ni/TiC. Note that the equilibrium coverage does not only depend on the formation energies of all species, but also on the lateral interactions between them and kinetic effects due to the interconnection of the possible elementary steps and correlations in the occupation of neighboring sites due to reactions. Kinetic models are thus required to appropriately account for the effect of the coverage. Finally, one can use the predicted coverage from the kMC simulations to re-calculate the PES at the new conditions, which would enable a better agreement between the kMC simulations and the predictions from the PES. Additional details on the coverage of surface species and number of product molecules produced during the initial stage of the reaction can be found in Figures S2 and S3, respectively.

A deeper analysis at the steady state event frequencies provides additional interesting insights into the reaction mechanism of the RWGS on Ni/TiC and about the main contributions of each region of the catalyst. Fig. 3b displays the event frequency plot at T = 550 K whereas information for the event frequency and coverages at all the temperatures studied are reported in Figure S4 and Table S5. Most H* species are formed over the Ni cluster in which only H_2 can adsorbs and dissociate, followed by a spillover of H* to the TiC region where it reacts with CO_2* to produce the COOH* intermediate. The role of the Ni cluster is, therefore, to facilitate hydrogenation reactions by dissociating H_2 and the subsequent spillover. The interface region produces some CO*, either via CO_2* dissociation or the COOH-mediated associative pathways, although to a much lesser extent than the TiC region. This is due to the high O* coverage that blocks available sites, as explained above. The contribution of the interface region increases with the reaction temperature, since the O* coverage is reduced. Last but not least, the TiC region is the main responsible for CO production, mainly via the COOH-mediated associative route because of the significant H* coverage (Table 1) that facilitates the COOH* formation. Note that CO_2* needs a free neighboring tC site to dissociate, an unlikely situation due to the high coverage, favoring the COOH-mediated associative pathway. This observation shows the importance of site availability and that it is necessary to consider free sites as actual reactants involved in the reaction. Note also that most of the water formation comes from the hydrogenation of OH* formed during the COOH* dissociation at the TiC region. A scheme of the overall reaction mechanism is illustrated in Fig. 3c, showing the synergy between the Ni cluster and the TiC surface, the former acting as a H* source and the latter using this H* to form COOH* and subsequently dissociating it to produce CO*. Moreover, the supported Ni cluster also changes the energetics of the neighboring Ti and C surface atoms (i.e., interface region), which can be very reactive at much higher temperatures (Fig. 3d), when the partial O* poisoning effect of the tTi sites is diluted.

3.3. Why is Ni/TiC much more active than TiC?

The analysis in the previous subsection shows that the TiC region dominates the RWGS reaction catalytic activity in Ni/TiC, which raises the question of why then TiC is two orders of magnitude less active than Ni/TiC. This controversy requires comparing kMC simulations for the two systems. Fig. 4a shows that the calculated turn over frequencies of both systems and the experimental ones [19] are in remarkable agreement, meaning that the chemistry of both systems is well captured by the kMC simulations employing the DFT derived rates. Nevertheless, some differences exist between the experimental systems and the theoretical model that are worth to note when aiming at a quantitative comparison. First, the Ni/TiC model corresponds to a Ni coverage of 0.14 ML, instead of the 0.10 ML coverage used in the experiments, and the experimental system corresponds to an ensemble of Ni clusters of different sizes and morphologies, while our model assumes that all clusters are flat and composed of 4 Ni atoms. Furthermore, additional deviations may arise from the limitations of the kMC method itself, errors in the computed DFT energetics or also in the truncation to two-body terms in the cluster expansion, which could be important at high surface coverages, among other limitations. These considerations explain why the agreement between kMC results and experiments is excellent for the RWGS on TiC(001) and just almost quantitatively correct for the Ni/TiC. In the TiC (001), the model closely approaches the real system, whereas in Ni/TiC, the complexity of the real system is not completely reproduced. In spite of these differences, the kMC simulations properly predict a much higher activity of the Ni/TiC system. In the following, we unveil the origin of this difference.

Fig. 4b shows that the dissociative pathway is responsible for most of the CO molecules produced on TiC, becoming even more dominant as the temperature rises. This is in contrast with the TiC region of Ni/TiC, in which the contribution of the dissociative route is practically negligible, with most of CO molecules produced from the COOH-mediated associative pathway. Since, for the relevant elementary steps, the energy barriers in either clean TiC or TiC region of Ni/TiC are the same, the natural question is where the calculated and experimentally observed difference in activity comes from. Again, the answer lies in the catalyst surface coverage, which plays a fundamental role. Table 2 shows that, on the clean TiC surface, only O* and CO_2* species have a significant coverage. Compared to the coverage of the TiC region in Ni/TiC (Table 1), we observe similar values for CO_2* but important differences for the O* and H*. At 550 K, the O* site occupancy of tC sites increases from 13 % for Ni/TiC to 46 % for TiC, while the H* site occupancy of h sites decreases from 35 % for Ni/TiC to 1 % for TiC. These differences are directly related to the change in the mechanism that drives the reaction, as the probability of some elementary reactions to be executed change with these magnitudes. The low H* coverage on clean TiC makes the COOH* formation more unlikely, decreasing not only the weight that the associative pathway has in comparison to the TiC region of Ni/TiC, but also drastically lowering the total TOF of the reaction. In spite of this, the event frequency plot shows that the COOH* formation step still occurs more times than the CO_2* dissociation, but in the vast majority of cases it goes backwards to CO_2* due to the low energy barrier of the reverse direction of only 0.26 eV (R15). Moreover, the high O* coverage on clean TiC also contributes to more COOH* going backwards to CO_2* due to its reaction with O* (i.e., COOH* + O* → CO_2* + OH*), further decreasing the overall TOF of the reaction. The direct CO_2* dissociation occurs less frequently, but this is a much more irreversible process: the energy barrier in the reverse direction is 1.08 eV (-R11), relatively high. Therefore, the net balance is higher for the dissociative pathway, making it the dominant reaction mechanism on clean TiC as schematically shown in Fig. 4c and as can be anticipated from the analysis of the PES. The event frequency and coverages at all the temperatures studies are reported in Figure S5 and Table S6.

The dominant reaction mechanism can change with temperature due to changes in the coverage, which can also be captured in kMC simulations. For instance, the amount of CO molecules produced from the dissociative pathway in the clean TiC surface

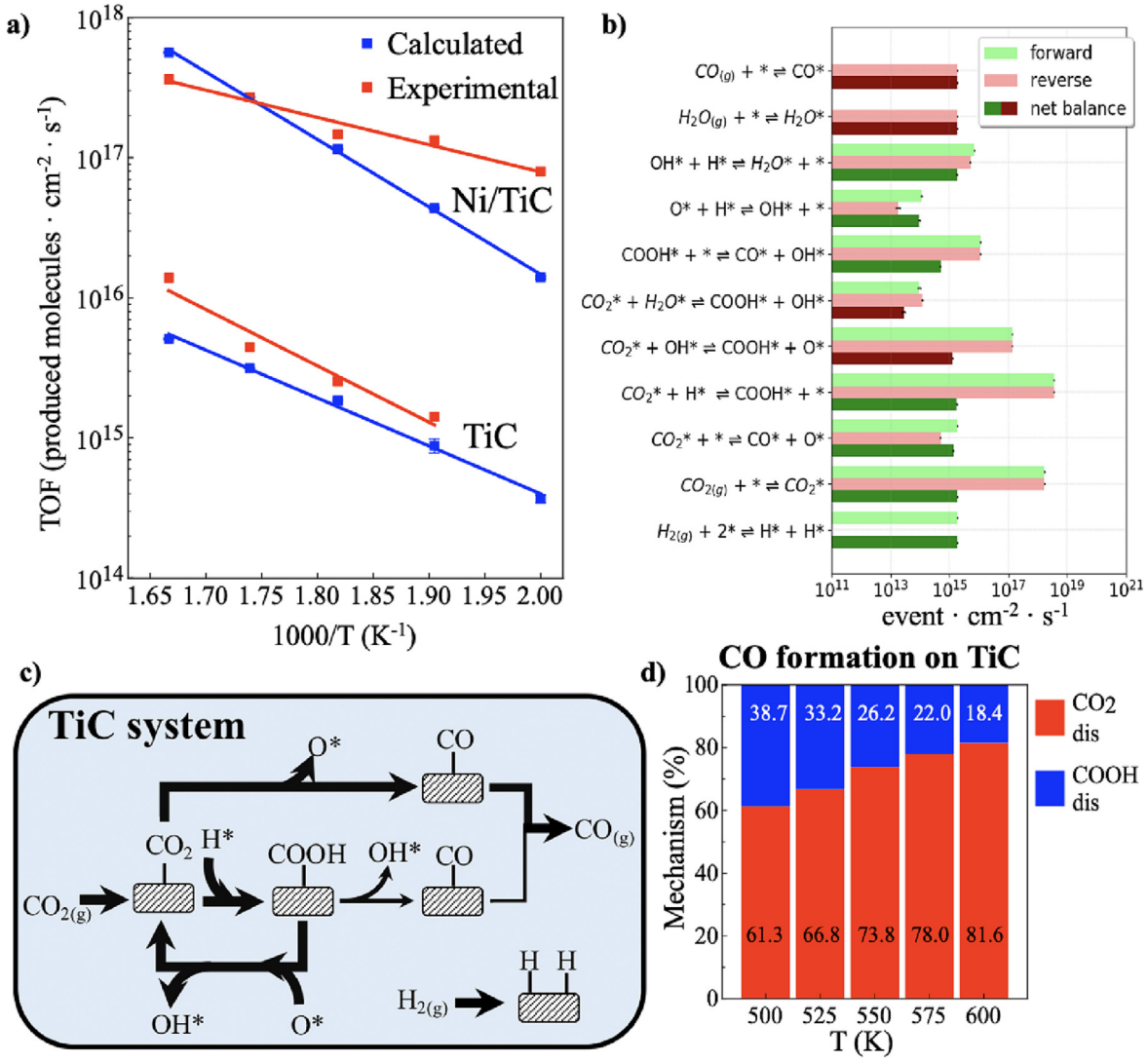

Fig. 4. a) Calculated and experimental (from ref. 19) turn over frequencies for the CO production at different temperatures for the TiC and Ni/TiC systems. b) Event frequency of the RWGS reaction on the TiC model at T = 550 K and P(H_2) = 4.5 bar and P(CO_2) = 0.5 bar. c) Scheme of the observed mechanism for the TiC model. d) Percentage of the dissociative and COOH-mediated pathways on the final CO production at five different temperatures.

Table 2
Percentage of site occupancy for the different species that are adsorbed on the TiC surface at 550 K under steady state conditions. Values of 0.0 represent an occupation lower than 0.05 % while dashes (-) means that this species cannot adsorb at that site.

T = 550 K	Site occupancy (%)		
Species	**tC**	**tTi**	**h**
CO*	0.0	–	–
O*	46.1	–	–
OH*	–	0.1	–
H_2O*	–	0.1	–
CO_2*	10.0	19.9	–
COOH*	0.2	0.4	–
H*	–	–	0.9
Total	**56.3**	**20.5**	**0.9**

increases from 61 % at 500 K to 82 % at 600 K (Fig. 4d). This change is directly related to the lower CO_2* and H* surface coverage at higher temperatures, hindering even more the COOH-mediated associative pathway. Note that the total coverage, in general, decreases with temperature, favoring unimolecular reactions over bimolecular ones. Finally, it is important to recall that the energetic interactions of reactants with neighboring spectator species can influence the energy barriers of elementary steps, as shown in Table S7. For instance, the energy barrier at the zero-coverage limit (i.e., obtained from DFT calculations with no spectator species) for COOH* dissociation to CO* + OH* in the TiC region is 0.50 eV (R29), but the average energy barrier computed by the cluster expansion in the kMC simulations is only 0.31 eV (550 K, Ni/TiC system). Since this is one of the most important elementary steps, this decrease has a significant impact in the overall TOF.

4. Conclusions

DFT calculations combined with kMC simulations have been performed to unravel the boost of activity experimentally observed for the RWGS reaction on Ni/TiC compared to TiC. The agreement between experimental and calculated data is remarkable and provides strong support to the conclusions that are derived from the present study. We show that, to a large extent, the conclusions that can be extracted from the analysis of the DFT potential energy surface coincide with those of the kMC simulations for the reaction taking place at the bare TiC surface. However, a completely different situation is found for the reaction at the more complex Ni/TiC

system. The analysis of the PES suggest that the dissociative pathway is the dominant reaction mechanism in all three regions of Ni/TiC, with the catalytic activity increasing in the order: TiC < interface < Ni, but spatially resolved kMC simulations point to the opposite direction, unveiling that CO is mainly produced in the TiC region via the COOH-mediated associative pathway. Moreover, kMC simulations show that the increased activity of Ni/TiC compared to TiC is not because of the lower energy barriers of many elementary steps on the Ni cluster, but due to a synergic effect between the supported Ni clusters and TiC. The former break H_2* to H*+H* much faster, and the H* spillover from the Ni clusters to the TiC region drastically boosts its catalytic activity towards the RWGS reaction. A surface poisoning of the Ni and interface regions at the initial stages of the reaction is responsible for the TiC region to be the active one as site blocking forbid reactivity on the Ni and interface regions, which is not possible to predict from the calculated PES.

While (free) energy profiles, mainly derived from DFT, have been instrumental in advancing our understanding of catalytic processes, they may be insufficient to come out with sound predictions or even to explain observations. Among other limitations, they do not easily account for the effect of surface coverage, which will require updating the potential energy surface for each situation, which becomes unpractical. Indeed, the present work shows that coverage effects and site blocking play a key role in determining the catalytic activity of the Ni/TiC system and it is likely that this conclusion will hold for complex catalysts that cannot be represented by an extended, almost perfect surface. This study highlights the importance of combining the electronic structure derived picture of the reactivity with kinetic modeling techniques, in particular kMC simulations, as a fundamental tool to delve deeper into the inner workings of complex catalytic systems, unravelling the role of complexity and developing a fundamental understanding towards the rational design of novel catalysts.

Data availability

The data used in this work have been made available on a public GitHub repository: https://github.com/plozanore/Surface_coverage_DFT_vs_kMC.

Declaration of Competing Interest

The authors declare that they have no known competing financial interests or personal relationships that could have appeared to influence the work reported in this paper.

Acknowledgments

The research at the Universitat de Barcelona has been supported by the Spanish Ministry of Science, Innovation and Universities (MICIUN) Spanish MCIN/AEI/10.13039/501100011033 PID2021-126076NB-I00 project, funded partially by FEDER Una manera de hacer Europa, and María de Maeztu CEX2021-001202-M grants, including funding from European Union and, in part, by and COST Action CA18234 by the Generalitat de Catalunya grant 2021SGR00079. PLR acknowledges MICIUN for a predoctoral FPU18/02313 grant. HPG acknowledges the funding received from the European Union's Horizon 2020 research and innovation programme under the Marie Skłodowska-Curie Grant Agreement No. 891756. Computational resources provided by Consorci de Serveis Universitaris de Catalunya (CSUC, former CESCA) with financial support from Universitat de Barcelona and Red Española de Supercomputación (grants QS-2020-1-0003 and QS-2020-2-0009) are gratefully acknowledged.

Appendix A. Supplementary material

Supplementary data to this article can be found online at https://doi.org/10.1016/j.jcat.2023.05.026.

References

[1] J.M. Thomas, W.J. Thomas, Principles and Practice of Heterogeneous Catalysis, VCH, Weinheim, 1997.
[2] M.A. Bañares, Operando methodology: combination of in situ spectroscopy and simultaneous activity measurements under catalytic reaction conditions, Catal. Today 100 (2005) 71–77.
[3] B.M. Weckhuysen, Determining the active site in catalytic process: operando spectroscopy is more than a buzzword, Phys. Chem. Chem. Phys. 5 (2003) 4351–4360.
[4] H. Topsøe, Developments in operando studies and in situ characterization of heterogeneous catalysts, J. Catal. 216 (2003) 155–164.
[5] A.D. Handoko, F. Wei, Jenndy, B.S. Yeo, Z.W. She, Understanding heterogeneous electrocatalytic carbon dioxide reduction through operando techniques, Nat. Catal. 1 (2018) 922–934.
[6] K. Feng, Y. Wang, M. Guo, J. Zhang, Z. Li, T. Deng, Z. Zhang, B. Yan, In-situ/Operando techniques to identify active sites for thermochemical conversion of CO_2 over heterogeneous catalysis, J. Energy Chem. 62 (2021) 153–171.
[7] Y. Li, S. Zhao, R. Tappero, U. Jung, A. Elsen, P.h. Baumman, R.G. Nuzzo, E.A. Stach, A.I. Frenkel, Complex structural dynamics of nanocatalysts revealed in operando conditions by correlated imaging and spectroscopy probes, Nat. Commun. 6 (2015) 7583.
[8] J. Goetze, I. Yarulina, J. Gascon, F. Kapteijn, B.M. Weckhuysen, Revealing lattice expansion of small-pore zeolite catalysts during the methanol-to-olefins process using combined operando X-ray diffraction and UV-vis spectroscopy, ACS. Catal. 8 (2018) 2060–2070.
[9] E.A. Walker, D. Mitchell, G.A. Terejanu, A. Heyden, Identifying active sites of the water-gas shift reaction over titania supported platinum catalysts under uncertainty, ACS. Catal. 8 (2018) 3990–3998.
[10] B. Kreitx, K. Sargsyan, K. Blöndal, E.J. Mazeau, R.H. West, G.H. Wehinger, T. Turek, C.F. Goldsmith, Quantifying the impact of parametric uncertainity on automatic mechanism generation for CO_2 hydrogenation on Ni(111), JACS Au 1 (2021) 1656–1673.
[11] A. Bruix, J.T. Margraf, M. Andersen, K. Reuter, First-principles-based multiscale modeling of heterogeneous catalysis, Nat. Catal. 2 (2019) 659–670.
[12] M. Pineda, M. Stamatakis, Kinetic Monte Carlo simulations for heterogeneous catalysis: fundamentals, current status, and challenges, J. Chem. Phys. 156 (2022).
[13] L. Grajciar, C.J. Heard, A.A. Bondarenko, M.V. Polynski, J. Meeprasert, A.E. Pidko, P. Nachtigall, Towards operando computational modeling in heterogeneous catalysis, Chem. Soc. Rev. 47 (2018) 8307–8348.
[14] A.H. Motagamwala, J.A. Dumesic, Microkineti33c modeling: a tool for rational catalyst design, Chem. Rev. 121 (2021) 1049–1076.
[15] J.A. Rodriguez, J.P. Ramírez, A.R. Gutierrez, Highly active Pt/MoC and Pt/TiC catalysts for the low-temperature water-gas shift reaction: effects of the carbide metal/carbon ration on the catalyst performance, Catal. Today 289 (2017) 47–52.
[16] H. Prats, M. Stamatakis, Atomistic and electronic structure of metal clusters supported on transition metal carbides: implications for catalysis, J. Mater. Chem. A 10 (2022) 1522–1534.
[17] P. Lozano-Reis, R. Sayós, J.A. Rodriguez, F. Illas, Structural, electronic, and magnetic properties of Ni nanoparticles supported on the TiC(001) surface, Phys. Chem. Chem. Phys. 22 (2020) 26145–26154.
[18] H. Prats, A.R. Gutiérrez, J.J. Piñero, F. Viñes, T.S. Bromley, J.P. Ramírez, J.A. Rodriguez, F. Illas, Room temperature methane capture and activation by Ni clusters supported in TiC(001): effects of metal-carbide interactions on the cleavage of the C-H bond, J. Am. Chem. Soc. 141 (2019) 5303–5313.
[19] J.A. Rodriguez, J. Evans, L. Feria, A.B. Vidal, P. Liu, K. Nakamura, F. Illas, CO_2 hydrogenation on Au/TiC, Cu/TiC and Ni/TiC catalysts: production of CO, methanol, and methane, J. Catal. 307 (2013) 162–169.
[20] P. Lozano-Reis, H. Prats, R. Sayós, J.A. Rodriguez, F. Illas, Assessing the activity of Ni cluster supported on TiC(001) toward CO_2 and H_2 dissociation, J. Phys. Chem. C 125 (2021) 12019–12027.
[21] J. Wellendorff, K.T. Lundgaard, A. Møgelhøj, V. Petzold, D.D. Landis, J.K. Nørskov, T. Bligaard, K.W. Jacobsen, Density functionals for surface science: Exchange-correlation model development with Bayesian error estimation, Phys. Rev. B. 85 (2012).
[22] G. Kresse, J. Hafner, Ab initio molecular dynamics for liquid metals, Phys. Rev. B. 47 (1993) 558–561.
[23] G. Kresse, J. Furthmüller, Efficient iterative schemes for ab initio total-energy calculations using a plane-wave basis set, Phys. Rev. B. 54 (1996) 11169–11186.
[24] G. Kresse, J. Furthmüller, Efficiency of ab-initio total energy calculations for metals and semiconductors using a plane-wave basis set, Comp. Mater. Sci. 6 (1996) 15–50.
[25] J.K. Nørskov, F. Studt, F. Abild-Pedersen, T. Bligaard, Fundamental Concepts in Heterogeneous Catalysis, Wiley, Hoboken, NJ, 2014.

[26] M. Stamatakis, D.G. Vlachos, A graph-theoretical kinetic Monte Carlo framework for on-lattice chemical kinetics, J. Chem. Phys. 134 (2011).
[27] M. Stamatakis, D.G. Vlachos, Unraveling the complexity of catalytic reactions via kinetic Monte Carlo simulation: current status and frontiers, ACS Catal. 2 (2012) 2648–2663.
[28] J. Nielsen, M. d'Avezac, J. Hetherington, M. Stamatakis, Parallel kinetic Monte Carlo simulation framework incorporating accurate models of adsorbate lateral interactions, J. Chem. Phys. 139 (224706) (2013) 1–13.
[29] H. Prats, S. Posada-Pérez, J.A. Rodriguez, R. Sayós, F. Illas, Kinetic Monte Carlo simulations unveil synergic effects at work on bifunctional catalysts, ACS Catal. 9 (2019) 9117–9126.
[30] A. Goswami, H. Ma, W.F. Schneider, Consequences of adsorbate-adsorbate interactions for apparent kinetic of surface catalytic reactions, J. Catal. 405 (2022) 410–418.
[31] X. Li, L.C. Grabow, Evaluating the benefits of kinetic Monte Carlo and microkinetic modeling for catalyst design studies in the presence of lateral interactions, Catal. Today 387 (2022) 150–158.
[32] S. Piccinin, M. Stamatakis, Steady-state CO oxidation on Pd(111): First-Principles kinetic Monte Carlo simulations and microkinetic analysis, Top. Catal. 60 (2017) 141–151.
[33] M. Jørgensen, H. Grönbeck, Scaling relations and kinetic Monte Carlo simulations to bridge the materials gap in heterogeneous catalysis, ACS. Catal. 7 (2017) 5054–5061.
[34] P. Lozano-Reis, H. Prats, P. Gamallo, F. Illas, R. Sayós, Multiscale study of the mechanism of catalytic CO_2 hydrogenation: role of the Ni(111) facets, ACS Catal. 10 (2020) 8077–8089.
[35] H. Prats, L. Álvarez, F. Illas, R. Sayós, Kinetic Monte Carlo simulations of the water gas shift reaction on Cu(1 1 1) from density functional theory based calculations, J. Catal. 333 (2016) 217–226.
[36] S. Piccinin, M. Stamatakis, CO oxidation on Pd(111): a first-principles-based kinetic Monte Carlo study, ACS Catal. 4 (2014) 2143–2152.
[37] L. Yang, A. Karim, J.T. Muckerman, Density functional kinetic Monte Carlo simulation of water gas shift reaction on Cu/ZnO, J. Phys. Chem. C. 117 (2013) 3414–3425.